Sensitivity of the Residual Circulation Diagnosed from the UARS data to the Uncertainties in the input Fields and to the Inclusion of Aerosols

Janusz Eluszkiewicz

Center for Meteorology and Physical Oceanography

Massachusetts Institute of Technology, Cambridge, MA 02139, U.S.A.

David Crisp

Earth and Space Sciences 1 Division

Jet Propulsion Laboratory, Pasadena, CA 91109, U.S.A.

R. G. Grainger and Alyn Lambert

Atmospheric, Oceanic, and Planetary Physics

University of oxford, Oxford OX 1 3PU, U.K.

Greenbelt, MD 20771, U.S.A.

A.E. Roche, J. B. Kumer, and J. 1,. Mergenthaler

Lockheed-Martin Palo Alto Research Laboratory

Palo Alto, CA 94304, U.S.A.

Submitted to *J. Atmos. Sci.*

July 11, 1996

Abstract

The simultaneous measurements of temperature, aerosol extinction, and of the radiatively active gases by several instruments onboard the *Upper Atmosphere Research Satellite* permit an assessment of the uncertainties in the diagnosed stratospheric heating rates and in the resulting residual circulation. In this paper, measurements taken by the Cryogenic Limb Array Etalon Spectrometer (CLAES) are used to compute the circulation and to compare it against values obtained previously from the measurements obtained by the Microwave Limb Sounder (MLS). There is a broad agreement between the two sets of calculations and known biases in either the CLAES or MLS measurements are found to be responsible for the areas of disagreement. The inclusion of aerosols has improved the estimates of the residual circulation in the lower stratosphere during the 1992-1993 period covered by CLAES, but a large uncertainty in these estimates is caused by the uncertainties in the assumed refractive indices for sulphuric acid solutions.

1 Introduction

Measurements acquired by the instruments onboard the *Upper Atmosphere Research Satellite (UARS)* have facilitated the estimation of the residual circulation at good vertical resolution over several seasonal cycles. In a previous publication (Eluszkiewicz et al. 1996, hereafter referred to as Paper 1) we have diagnosed the circulation for the September 1991 - August 1994 period using fields of temperature and of radiatively active gases measured mainly by the "Microwave Limb Sounder (MLS) onboard *UARS*. In the middle and upper stratosphere, we identified several interesting phenomena, including the semiannual and quasi-biennial oscillations in the Tropics, the interhemispheric asymmetry in the downward velocities between the northern and southern winters, and the relation of these velocities to the wave forcing diagnosed as the residual in the momentum equation. We also attempted to provide quantitative estimates of the circulation in the lower stratosphere, but were hampered by the vertical range of MLS temperature measurements (which only extend clown to 22 hPa in the Version 3 data we used) and by the known biases in the ozone measurements (in particular, the low bias at 46 hPa in the Tropics and large systematic errors at 100 hPa). In addition, while the radiative effects of Mt. Pinatubo aerosols were assessed for a few selected profiles using measurements taken by the Improved Stratospheric and Mesospheric Sounder (ISAMS) onboard *UARS*, these effects were not included in the zonal-mean fields of diabatic heating, thus leading to large uncertainties in the circulation diagnosed for the 1991-1992 period.

In this paper, the residual circulation will be diagnosed using data obtained by another *UARS* instrument, the Cryogenic Limb Array Etalon Spectrometer (CLAES). The input fields are described in section 2. In sections 3 and 4, the diagnosed heating rates and the residual circulation are described and compared with the results from Paper 1. In section 5, we discuss the effects of including the aerosols in the heating calculations. A summary of the results is given in section 6.

2 Input Data

The zonally averaged fields of temperature, temperature tendency, ozone (from blocker 9), methane, nitrous oxide, and aerosol extinction used in the heating calculations have been obtained from the CLAES Version 7 Level 3A L files available on Compact 1 Disc Rea d-Only Memory from the NASA Goddard Distributed Access Archive Center (it was found in Paper I that the use of Level 3AL files, as opposed to mapped products, leads to small errors n the zonal-méan fields of diabatic heating). The averaging periods considered are listed in Table . They differ slightly from the corresponding periods in Table 2 of Paper 1, because the periods in that paper were chosen to be as close to the yaw days as possible (to ensure a near-simultaneity of the resulting quasi-global fields) and because the door of the CLAES instrument was closed for a couple of days prior to and after each yaw maneuver. The CLAES fields are augmented by the MLS distribution of water vapor (since CLAES Version 7 water vapor data are not recommended for scientific use by the instrument team) and by the LIMS daytime distribution of NO_2 extended to a full seasonal cycle on the assumption of hemispheric symmetry for the respective season. The tropospheric CO_2 mixing ratio is computed by means of the expressions given by Keeling at al. (1 989) and a stratospheric CO_2 concentration of 346 ppmv on January 1, 1993 is assumed. The treatment of tropospheric clouds, surface al bedo, and solar fluxes at the top of the atmosphere is described in Paper 1.

The primary aerosol product used in this paper are the zonal-mean distributions of extinction at 780 cm^{-1}. The choice of this wavenumber among several others at which CLAES measures aerosol extinction was motivated by the results described in Mergenthaler et al. (1 995). To - gether with the fields of temperature and water vapor, these measurements allow us to infer the wavelength-dependent extinction and scattering coefficients and the asymmetry parameter at nine UARS vertical levels equally spaced in log-p ressure between 100 and 4 hPa, using the method described by Grainger et al. (1 995, 1996). in section 5 we will present results describing the very

good agreement in the aerosol optical depths and the resulting heating rates between CLAES and ISAMS (for the evaluation of the CLAES and ISAMS aerosol measurements, see Massie et al. 1996 and Lambert et al. 1996, respectively). A major uncertainty in assessing the aerosol heating effects is caused by the uncertainties in the refractive indices for H_2SO_4 (Grainger et al. 1995).

3 Heating Rates

The comprehensive radiative transfer model used in the heating calculations has been been described in a series of previous publications (Crisp 1986, 1989, 1 990; Santee 1 993; Santee and Crisp 1 993; Gerstell 1 995; Gerstell et al. 1 995; Paper I). It includes all radiative processes known to be important in the atmosphere, i.e., absorption, emission, and multiple scattering by gases, clouds, and aerosols, and is well suited for studying the difficult lower stratosphere region. The heating calculations are performed on a grid with 61 vertical levels equally spaced in log-pressure between the ground and 0.01 hPa. This resolution is twice that of the CLAES retrievals. The CLAES data are linearly interpolated in log-pressure to provide values at the finer grid resolution. The meridional spacing in the calculations is 5°.

The heating rates (with aerosols excluded) for two solstice months are shown in Figure 1, together with the corresponding fields diagnosed from MLS data, 'J'here is an overall agreement between the two sets of calculations, at least for pressures less than I () hPa. In particular, both the CLAES- and MLS-based heating rates have regions of strong cooling in the winter hemisphere (with very similar magnitudes), weak cooling in the summer hemisphere, and heating in the Tropics. There is about 1 K day^{-1} more heating in the CLAES fields above 1 hPa, 1 K day^{-1} less heating between 1 and *2 h* 'a, and ().5 day--' more heating between 2 and 3 h} 'a. These differences are related to the systematic differences between the CLAES and MLS O_3 fields (Cunnold et al. 1996). In addition, the systematic low bias in CLAES temperatures between 2 and 3 hPa (Gille et al.

1996) leads to less IR cooling and thus enhanced net heating in this pressure range.

Larger differences between the CLAES- and MLS-based heating fields occur in the lower stratosphere. Note in particular the region of net cooling at 46 hPa in the Tropics in the MLS field in January and its absence in the CLAES calculation. It was noted briefly in Paper I that the net tropical heating rates diagnosed from MLS data decrease above 100 hPa, occasionally reaching negative values at 46 hPa before starting to increase at higher altitudes (see Figures 3 and 12 in Paper 1). Similar behavior was noted by other researches (K. Rosenlof as quoted by Brock et al. 1995) and it has consequences for the modeling of tracers (S. Wofsy, personal communication 1995). We believe that the clip between 100 and 46 hPa was mainly the result of the tropical O_3 values measured by MLS being systematically too low at 46 hPa (Froidevaux et al. 1996), as it is not present when the O_3 values measured by CLAES are used in the heating calculations, even when aerosols are either present at low abundances or ignored. To illustrate this, the equatorial ozone and heating profiles for January 1992 are shown in Figure 2. Note in particular the underestimate in the MLS O_3 mixing ratio at 46 hPa and the corresponding features in the profiles of solar and net heating. The inclusion of aerosols (which are discussed in more detail in section 5) increases the heating rates, but dots not eliminate the 46-hPa minimum in the MLS-derived profile of net heating. Figure 2 also suggests that until the 46-hPa problem is removed in future versions of MLS ozone retrieval algorithm, an approximate method of eliminating its effect on the tropical heating profiles would be to ignore the 46-hPa level and interpolate the heating rates between 100 and 22 hPa (where the MLS- and CLAES-derived profiles are in close agreement). We also note in Figure 2 the sensitivity of the IR cooling rates to the assured temperature profile, with temperature differences on the order of 1 K causing differences in the diagnosed heating rates of about 0.1 K day^{-1} (a similar sensitivity was noted previously by Olaguer et al. 1992). This is further illustrated in Figure 3a, which shows the differences between the CLAES and MLS ozone and temperature fields

and between the diagnosed heating rates (without aerosols). The temperature effect is larger than the ozone effect, but peaks at a somewhat lower altitude (56 hPa, midway between the 46 and 68 hPa CLAES retrieval levels), thus leaving MLS ozone as the primary cause of the heating minimum at 46 hPa. In addition, CLAES ozone may be systematically high in the lower stratosphere (Bailey et al. 1996), thus leading to more solar heating. However, the differences between the MLS and CLAES fields shown in Figure 3a may be different at other times; in particular there is evidence that the low bias in the MIS ozone at 46 hPa diminishes with time (Froidevaux et al. 1 996), with the corresponding decrease in the bias in the solar heating (see Figure 3b). As for temperature, it is interesting that differences on the order of a few K between the CLAES and National Meteorological Center (NMC) temperatures (used in the MLS Version 3 files for p $\geq$ 46 hPa) exist even between 100 and 10 hPa where he CLAES temperatures are constrained to the NMC values (Gille et al. 1996).

4 Residual Circulation

Figures 4-7 and Figure 9 show the global distributions of the zonal wind $\bar{u}$, the mass-weighted streamfunction X*, the meridional and vertical components of the residual circulation $(\bar{v}^*, \bar{w}^*)$, and the momentum residual, respectively. Figure 8 illustrates the variability of the input fields and of the circulation at the equator. The method of calculating these fields and tile format of the figures are identical to those in Paper 1, thus allowing a direct comparison. The residual circulation is computed from the heating fields using a streamfunction approach (Santee and Crisp 199.5), with the lower and upper boundary conditions (at 100 and 0.1 hPa, respectively) introduced self-consistently with the diagnosed heating rates. The requirement of global mass balance at each pressure level is satisfied by solving the streamfuction equation to within an additive height-dependent number.

4.1 $\bar{u}$

The distributions of zonal wind are qualitatively similar to those presented in Figure 6 of Paper 1. Wintertime westerlies are weak in January 1992 and February 1993 as a consequence of stratospheric warmings (note the patch of easterlies at high northern latitudes above 1 hPa in January 1992). The final warming (the transition to summertime easterlies) occurs in March-April and in October-November in the northern and southern hemisphere, respectively. The summertime easterlies are very strong in the subtropical stratopause region. In the tropics, there are some differences between the distributions presented here and those shown in Paper 1. In particular, the semiannual oscillation (SAO) easterlies are stronger in March-May 1992 (for example, in excess of 50 m s^{-1} around 2 hPa in March compared to less than 20 m s^{-1} in Paper 1). Also, the quasi-biennial oscillation (QBO) westerlies at the end of 1992 and the beginning of 1993 are much stronger than in Paper 1. These stronger winds will be shown more clearly in Figure 8 below.

4.2 X^* and $\bar{v}^*$

The summer branch of the Brewer-Dobson circulation is much more vigorous than in Paper 1. In particular, the regions of positive X^* in the southern hemisphere in January-February 1992 and in January 1993 have been greatly reduced or have disappeared completely. Reflecting more realistic ozone mixing values used in the heating calculations, the circulation is smoother around 46 hPa in the Tropics (note in particular the absence of the sharp wedge-like pattern in the northern subtropics in March 1992). As in Paper I, the southern branch of the circulation intrudes into the northern hemisphere around the stratopause in March of both years.

Among the similarities in the distributions of $\bar{v}^*$ shown here and those presented in Paper I of particular note are the strong poleward winds in the winter hemisphere in the stratopause region, meridional winds of less than 0.5 m s^{-1} throughout most of the middle and lower stratosphere,

and regions of equatorward flow around 46 hPa in the summer (southern) hemisphere in the two Januaries; in January and February 1992 there are also regions of summertime equatorward flow around 10 hPa. The differences include the much weaker poleward flows in the southern hemisphere lower mesosphere in October-November 1992, the absence of a double-peakecl structure in the region of strong poleward winds in the northern hemisphere in January 1992 (with these winds being stronger than in Paper 1), and a generally smoother structure in the upper stratosphere and lower mesosphere.

4.3 $\bar{w}^*$

The wintertime downwelling at high latitudes is strong during disturbed periods (compare for example January 1992 with January 1993), reaching magnitudes in excess of 12 mm s^{-1} in January 1992. In the mesosphere, the maximum downward velocities in the southern hemisphere in August 1992 are larger than their northern counterparts in the two Februaries. In the stratosphere, wintertime downward velocities are larger in the north, with the exception of the January 1993 period (when velocities are comparable to those at high southern latitudes in July 1992). In the lower stratosphere, velocities arc smaller than 1 mm s^{-1} during tile southern winter 1992, but exceed 2 mm s^{-1} in high northern latitudes during the disturbed periods of January 1992 and February 1993. During July and August 1992, the wintertime descent maximizes away from the pole in the lower portions of the stratosphere (note in particular the -2111111 s^{1} contour).

Downwelling in high latitudes occurs during equinoctial months, but is stronger in the spring hemisphere. Consistent with the persistence of a well-orga]lizcd polar vortex and a later final warming in the southern hemisphere, the springtime downwelling is stronger in the south (compare the southern latitudes in October-Novcml~er 1992 with the northern latitudes in April-March 1992; also, September 1992 with March 1992 in the upper stratosphere and lower mesosphere). These

results are in line with the findings of Paper I

In the summertime, high-latitude downward velocities in the stratosphere are always smaller than 0.5 mm s^{-1} and are somewhat stronger in the southern hemisphere. As in Paper I, upward velocities in the summertime upper stratosphere and lower mesosphere maximize in mid-latitudes rather than at the pole. In fact, the high-latitude downwelling region extends all the way to 0.46 hPa in the summer (southern) hemisphere during the two Februaries and in January 1 993, whereas in Paper 1 it extended only to about 1 hPa.

In the Tropics, a region of downwelling exists in the upper stratosphere and lower mesosphere during northern and southern winters, with the downward velocities being stronger during northern winter. This region expands downward from a level in the mesosphere between January and February of both years and possibly between July and August 1992. Paper I discusses these velocities in the context of SAO. As in Paper I, large downward velocities (in excess of 2 mm s^{-1}) persist at the tropical stratopause into March 1993 and the SAO downward velocities in March of both years exceed those in September 1992. The upward velocities underlying the SAO downward velocities are somewhat stronger than in Paper 1 (e. g., in excess of 4 mm s^{-1} at 2 hl'a in January 1993, compared with about 3 mm S–l in Paper I).

To illustrate the tropical variability more clearly, we show in Figure 8 the equatorial time-height sections of temperature, ozone, zonal wind, methane, nitrous oxide, and vertical velocity. Compared with the results shown in Figure 12 of Paper], we note an overall similarity in the SAO signal, including the asymmetry in the maximum vertical velocities (both positive and negative) between the northern and southern winters. This asymmetry may be responsible for the asymmetry between the two SAO phases in the distributions of tracers, with both CH_4 and N_2O negative anomalies exhibiting lower values during May-June than during November-December 1992, although a quantitative link between the SAO in $\bar{w}^*$ and in tracers has proved difficult to establish (Solomon et al.

1986, Gille et al. 1987). As in Paper 1, the SAO upwelling during the northern winter phase in 1992 is stronger than in 1993. There are also indications of a QI1O signal in the middle and lower stratosphere, but this signal is different from its counterpart in Paper 1, with the westerlies around 10 hl'a being weaker in early 1992 and stronger at 30 hPa in late 1992. The QBO-like (i.e., one that follows the pattern in $\bar{u}$) signature in the ozone field is in opposite phase to that in Paper 1, with low O_3 anomalies being in phase with positive temperature anomalies. This behavior is contrary to expectations (Hasebe 1994) and gives rise to negative vertical velocities between 10 and 30 hPa in 1992. These negative velocities are underlain by the large upwelling (in excess of 0.5 mm s^{-1}) caused by Mt. Pinatubo aerosols (see discussion in section 5).

4.4 Momentum residual

The values of the residual at mid- and high latitudes are similar to those in Paper 1, but exhibit a somewhat smoother structure, consistent with the smoother structure in the diagnosed $\bar{v}^*$ field. As in Paper 1, the largest values of the residual are found at high northern latitudes in January 1992 (more than 30 m s^{-1} day^{-1} at the stratopause). The values of the residual in tile upper stratosphere and lower mesosphere are smaller during the Southern winter of 1992 than during tile two northern winters, but, they increase as the season progresses from early to late winter and in September 1992 are larger than their northern counterparts (however, the situation is reversed in the middle and lower stratosphere). In January 1993, the values of the residual are similar to those diagnosed by Rosenlof (1 995) (see her Figure 7), who used a different radiation code with MLS ozone and United Kingdom Meteorological Office temperatures as input. For example, our values around 1 hPa in the northern hemisphere are between 15 and 20 m s^{-1} day^{-1} compared with Rosenlof's 15 m s^{-1} $clay^{-1}$; note also the presence in both studies of a region of positive residual around 4 hPa at high northern latitudes and the positive values in the southern hemisphere at the

stratopause and around 46 hPa.

5 Aerosol Heating

Following the eruption of Mt. Pinatubo in June 1991, there was a period of significantly enhanced aerosol concentrations in the stratosphere. The radiative heating effects of Pinatubo aerosols were computed in Paper 1 for a few selected ISAMS profiles spanning a range-of latitudes and times. It was found, in agreement with previous studies, that the main effect is in the thermal infrared, where the cooling rates become less negative (by up to 0.5 K day^{-1}) due to the absorption of the upwelling radiation from the warm troposphere. In contrast, the solar heating effects were much smaller (less than 0.1 K day^{-1}) as a result of the very small absorptivity in the visible part of the spectrum for the assumed pure sulphate composition. However, the magnitude of aerosol heating in Paper I was different from the values obtained in other studies. For example, the maximum thermal heating effect was almost twice as large as that presented in 'Table 2 of Kinne et al. (1992) and in Figure 5 of Kinnison et al. (1994) for Mt. Pinatubo, but both the solar and the thermal aerosol heating rates from Paper I were significantly smaller than the values shown in Figure 1 of Gerstell et al. (1995) (the latter studied the period following the eruption of El Chichón using the same radiation code as used here). The reason for these discrepancies are the different vertical profiles of aerosol extinction assumed in these studies. Both Kinne et al. and Gerstell et al. used the observed (and comparable) column optical depths and distributed them in the vertical assuming a constant (height-independent) and a Gaussian distribution, respectively. In Figure 10. we show that for the same assumed total optical depth, the shape of the profile has a dominant effect on the magnitude of the heating (simply because a more peaked vertical distribution of aerosol extinction gives rise to a more peaked distribution of the heating). The effect of the vertical location of tile extinction peak is smaller, thus demonstrating little shielding influence of ozone

or other gases. These results demonstrate the importance of an accurate knowledge of the aerosol vertical profiles in the heating calculations and the advantage provided in this regard by the aerosol measurements carried out by the *UARS* instruments. As shown in Figure 11, the lat ter agree among themselves to a remarkable degree and this gives us an additional reason to be confident in the magnitude of the aerosol heating effects we calculate.

The global aerosol heating effects are shown in Figure 12. This figure demonstrates that a arge uncertainty in evaluating these effects is caused by the uncertainties in the assumed refractive ndices for sulphuric acid solutions. In the current study, values of the imaginary component of the refractive index measured by Palmer and Williams (1 975) have been normalized to the more accurate measurements of Rei nsberg et al. (1974). The original Palmer and Williams values give more absorption shortward of 12 μm, increasing the net aerosol heating by more than 0.2 K day^{-1}, with significant heating even in the solar part of the spectrum (at wavelengths longer than 2.7 μm).

The time series of the aerosol-induced heating and upwelling at the equator is shown in Figure 13. The aerosol effects diminish with time due to particle sedimentation and latitudinal spreading, hut remain significant into 1993. The enhanced aerosol heating at 100 hPa is caused by the presence of tropospheric clouds, which are not distinguished from the sulphate aerosol in CLAES Version 7 data.

Finally, in Figure 14 we present the seasonally-averaged vertical velocity at 100 hPa, which is used to derive the values for the extratropical mass fluxes shown in Table 2. Compared with the results presented in Paper 1 (Figure 5 and Table 3, respectively), the extratropical downwelling is much stronger at all seasons in both hemispheres; note in particular the large (more than 0.7 mm s^{-1}) downward velocities during southern winter (in fact, maximum velocities during southern winter exceed those during northern winter). A pec uliarity of Paper I were the small mass fluxes computed in the summer hemisphere, in line with the results obtained by Rosenlof (] 995) (see the

numbers for the 70-hPa level in her ~'able 1; wc assume that the values at 100 hl'a would be roughly 30% larger). These fluxes are much larger now, e.g., the southern hemisphere flux during December-January-February has increased from 14 to 37-46 x 108 kg S-*. The differences arc related to the differences in the CLAES and NMC temperature fields, as the diagnosed circulation is very sensitive to even small temperature differences (see Figure 3 above). The inclusion of aerosols has a smaller effect on the mass fluxes. Somewhat surprisingly, the mass fluxes for the northern winter are only slightly larger than for the southern winter, contrary to the results obtained in earlier studies (Yang and Tung 1996 and references therein), which indicated a much greater contrast (almost a factor of 2) between the two hemispheres. A robust feature of this study, consistent with the results obtained by Rosenlof (19%5), is the latitudinal extent of the "extratropics," with the region of negative $\bar{w}^*$ extending to lower latitudes in the winter compared with the summer hemisphere and during the southern summer compared with the northern summer.

6 Summary

The gross features in the fields of diabatic heating and of the associated residual circulation diagnosed from CL AES measurements are remarkably similar to the fields diagnosed using MLS data as input. In particular, both sets of calculations demonstrate the semiannual oscillation (SAO) in the tropical upper stratosphere and lower mesosphere, with vertical velocities during the northern winter phase being stronger than the velocities during the southern winter period. Stronger SAO velocities arc diagnosed for the northern winter of 1992 than for the northern winter of 1993. The SAO velocities in the upper stratosphere arc somewhat stronger in the CL AES-derived fields, as a result of larger diagnosed heating rates (caused by biases in the CL AES ozone and temperature measurements). The CL AES-derived fields arc smoother above the stratopause, mainly because the MLS temperature gradients above 1 hPa arc too steep. Apart from that region, the two fields

agree even quantitatively at pressures less than 10 hPa.

Large disagreements between the CLAES- and MLS-derived circulations occur in the lower stratosphere. The minimum in the vertical velocity at 46 hPa in the Tropics diagnosed from *MIS* data is not present in the CLAES-based fields; instead there is tropical downwelling between 10 and 30 hPa in early 1992. This downwelling is caused by low values of ozone measured by CLAES. The circulation in the lower stratosphere is quite sensitive to the assumed temperature fields, with temperature differences on the order of 1 K causing differences of about 0.1 K day^{-1} in the diagnosed heating rates. As a result of small differences in temperature between CLAES and NMC, the extratropical mass fluxes are much larger in the CLAES circulation.

The most important improvement in the circulation diagnosed from CLAES data is the inclusion of the effects of Mt. Pinatubo aerosols. The aerosol heating is very sensitive to the assumed vertical profile of aerosol extinction and the global aerosol measurements by the *UARS* instruments lead to more realistic estimates of this heating. However, the uncertainties in the assumed refractive indices for H_2SO_4-H_2O solutions continue to be a major source of uncertainty in these estimates. CLAES measurements indicate that aerosol heating was significant as late as early 1993. Preliminary results from the Caltech/JPL two-dimensional model suggest that the inclusion of the aerosol contribution to net heating improves simulations of total Ozone (Yuk Yung, personal communication 1996), although a completely satisfactory simulation of total ozone based on UARS data is not possible, given the sensitivity of the column ozone to the circulation in the 100-300 hPa region and the restriction of UARS data to pressures less than 100 hPa.

Clearly, the estimates of the residual circulation are still fraught with large uncertainties, but with the advent of *UARS* measurements these uncertainties are being reduced. Future work in this area using improved versions of *UARS* retrieval algorithms is planned.

Acknowledgments

Communications with M. Gerstell and S. Kinne helped us to understand the aerosol heating effects better. M. Santee provided the streamfunction c.ode, A. Dessler is thanked for his efforts in providing CLAES NO_2 fields, even though at this stage we have chosen to continue using the LIMS fields. Y. Yung, E. Chang, and E. DeJong are thanked for the use of their computer facilities. This research was carried out at MIT as part of the UARS Guest Investigator program under NASA grant NAG5-2812. Oxford authors acknowledge funding by the Natural Environment Research Council.

References

Bailey, 1'. 1,., D. 1'. Edwards, J. C. Gille, L. V. Lyjak, S. T. Massie, A. E. Roche, J. B. Kumer, J. L. Mergenthaler, B. J. Connor, M. R. Gunson, J. J. Margitan, 1. S. McDermid, and T. J. McGee, 1996: Comparison of cryogenic limb array etalon spectrometer (CLAES) ozone observations with correlative measurements. *J. Geophys. Res.*, 101, 9737 -9'756.

Brock, C. A., P. Hamill, J. C. Wilson, H. 11. Jonsson, K. R. Chan, 1995: l'article formation in the upper tropical tropopause: A source of nuclei for the stratospheric aerosol. *Science*, 270, 1650-1653.

Crisp, D., 1986: Radiative forcing of the Venus mesosphere. 1. Solar fluxes and heating rates. *Icarus*, **67**, 484-5]4.

Crisp, D., 1989: Radiative forcing of the Venus atmosphere. 11. Thermal fluxes, cooling rates, and radiative equilibrium temperatures. *Icarus*, 77, 391-413.

Crisp, D., 1990: Infrared radiative transfer in the dust-free martian atmosphere. *J. Geophys. Res.*, 95, 14,577 -]4,588.

Cunnold, D. M., L. Froidevaux, J. M. Russell, B. Connor, and A. Roche, 1996: Overview of UARS ozone validation based primarily on intercomparisons among UARS and Stratospheric Aerosol and Gas Experiment II measurements. *J. Geophys. Res.*, 101, 10,335-10,350.

Eluszkiewicz, J., D. Crisp, R. Zurek, L. Elson, E. Fishbein, L. Froidevaux, J. Waters, R. Grainger, A. Lambert, R. Harwood, and G. Peckham, 1996: Residual circulation in the stratosphere and lower mesosphere as diagnosed from Microwave Limb Sounder data. *J. Atmos. Sci.*, 53, 217-240.

Froidevaux, L. and coauthors, 1996: Validation of UARS Microwave Limb Sounder ozone measurements. *J. Geophys. Res.*, **101**, 10,017-10,060.

Gerstell, M. T., 1995: *Two radiative transfer models with terrestrial applications.* Ph. D. thesis (Part 1), California Institute of Technology, Pasadena.

Gerstell, M. F., J. Crisp, and D. Crisp, 1995: Radiative forcing of the stratosphere by SO_2 gas, silicate ash, and H_2SO_4 aerosols shortly after the 1982 eruptions of El Chichón. *J. Clim.*, **8**, 1OGO-107O.

Gille, J. C., L. V. Lyjak, and A. K. Smith, 1987: The global residual mean circulation in the middle atmosphere for the northern winter period. *J. Atmos. Sci.*, **44**, 1437-1 452.

Gille, J. and coauthors, 1996: Accuracy and precision of cryogenic limb array etalon spectrometer (CLAES) temperature retrievals. *J. Geophys. Res.*, 101,9583-9601.

Grainger, R. G., A. Lambert, C. D. Rodgers, F. W. Taylor and q'. Deshler, 1995: Stratospheric aerosol effective radius, surface area and volume estimated from in frared measurements. *J. Geophys. Res.*, 100, 16,507-16,518.

Grainger, R. G., A. Lambert, C. D. Rodgers and F. Taylor, 1 996: Properties of the Mt. Pinatubo Aerosol cloud determined from ISAMS measurements at 12.1 μm. In *Proc. NATO Advanced Research Workshop, The Effects of the Mt. Pinatubo Eruption on* the A *tmosphere and Climate*, Rome, Italy, Sept. 26-30, 1994, Springer-Verlag, Berlin (in press).

Hasebe, T., 1994: Quasi-biennial oscillations of ozone and diabatic circulation in the equatorial stratosphere. *J. Atmos. Sci.*, **51**, *729-74,5.*

Keeling, C. D., R. B. Bacastow, A. F. Carter, S. C. Piper, 'J'. T'. Whorf, M. Heiman, W. G. Mook, and 11. Roeloffzen, 1989: A three-dimensional model of atmospheric CO_2 transport based on

observed winds: 1. Analysis of observational data. In Aspects *of Climate Variability in the Pacific and Western Americas,* edited by D. 11. Petersen, Geophysical h'monographs 55, pp. 165-236, American Geophysical Union, Washington , D. C.

Kinne, S., O. B. Toon, and M. J. l'rather, 1992: Buffering of the stratospheric circulation by changing amounts of tropical ozone: A Pinatubo case study. *Geophys. Res. Lett.,* 19, *1927-1930.*

Kinnison, D. E., K. E. Grant, 1'. S. Connell, D. A. Rotman, and D. J. Wuebbles, 1994: The chemical and radiative effects of the Mount Pinatubo eruption. *J. Geophys. Res.,* 99, 25,705 - *25>731.*

Lambert, A., R. G. Grainger, J. J. Remedios, W. J. Reburn, C. D. Rodgers, F. W. Taylor, A. E. Roche, J. B. Kumer, S. 'I'. Massie and T. Deshler, 1996: Validation of aerosol measurements from the improved stratospheric and mesospheric sounder. *J. Geophys. Res.,* 301,9811-9830.

Massie, S. 'I'. and coauthors, 1996: Validation studies using multiwavelength Cryogenic Limb Array Etalon Spectrometer (CLAES) observations of stratospheric aerosol. *J. Geophys. Res.,* 101, *9757-9773.*

Mergenthaler, J. L., J. B. Kumer, and A. E. Roche, 1995: CLAES observations of Mt. Pinatubo stratospheric aerosol. *Geophys. Res. Lett.,* 22, 3497-3.500.

Olaguer, E. 1'., H. Yang, and K. K. Tung, 1992: A reexamination of the radiative balance of the stratosphere *J. Atmos. Sci.,* 49, 1242-1263.

Remsberg, E. E., D. Lavery, and B. Crawford, 1974: Optical constants for sulfuric and nitric acids. *J. Chem. Eng. Data,* **19,** *263-265, 1974.*

Rosenlof, K. 11., 1995: Seasonal cycle of the residual mean meridional circulation in the stratosphere. *J. Geophys. Res.*, **100**, 51 *73-5191!*

Santee, M., 1993: *The thermal structure, dust loading, and meridional t ransport in the martian atmosphere during late southern summer.* Ph.D. thesis, California Institute of Technology, Pasadena.

Santee, M. L. and D. Crisp, *1993:* Thermal structure and dust loading of the martian atmosphere during late southern summer: Mariner 9 revisited. *J. Geophys. Res.,* 98, 3261-3279.

Santee, M. L. and D. Crisp, 1995: Diagnostic calculations of the circulation in the martian atmosphere. *J. Geophys. Res.*, **100**, *5465-5485.*

Solomon, s., J. T. Kiehl, R. R. Garcia, and W. Grose, 1986: Tracer transport by the diabatic circulation deduced from satellite observations. *J. Atmos. Sci.,* 43, 1603-1617.

Yang, 11. and K. K. Tung, 1996: Cross-isentropic stratosphere-troposphere exchange of mass and water vapor. *J. Geophys. Re s.,*] 01, 9413-9123,

'J'able 1

Averaging Periods for Radiative Heating and Residual Circulation Calculations.

Yaw	Label	Averaging Periods (South- & North-viewing)
4	Jail 92	January 15-22 & January 6-13, 1992
5	Feb 92	February &13 & February 15-22, 1992
G	Mar 92	March 24-31 & March 15-22, 1992
7	A-M 92	April 23-3(I & May 2-9, 1992
8	M-J 92	June 15-22 & May 24-31, 1992
9	Jul 92	July 5-1? & July 18-25, 1992
10	Aug 92	August 14-21 & August 5-12, 1992
11	Sep 92	September 1 3-20 & September 22-29, 1 992
12	0-N 92	October 30- November 6 & October 21-28, 1992
13	N-D 92	November 21-28 & November 30- December 6, 1992
14	Jan 93	January 10-17 & January 1-8, 1993
15	Feb 93	February 1-8 & February 10-17, 1993
16	Mar 93	March 20-27 & March 11-18, 1993
17	A-M 93	April 21-25 & April 27- May 4, 1993

Table 2

Extratropical Downward Mass Flux at 100 hPa (in 10^8 kg s^{-1})

	Winter				Summer			
	No Aer	P-W/R	P-W	Lat	No Aer	P-W/R	P-W	Lat
NH	95	105	I 09	30	16	25	28	40
SH	85	96	101	25	37	44	46	45

Note: The averaging periods are DJF and JJA as appropriate for the season and hemisphere indicated. The extratropics are defined as the region poleward of the lowest latitude at which the vertical velocity is downward (see Figure]4). This latitude is given in the "], at" column. "No Aer" is the estimate without aerosols, whereas "P-W/}{" and "P-W" refer to the estimates with aerosols, assuming the normalized and the original Palmer and Williams refractive indices for sulphuric acid, respectively.

Figure captions

Figure 1. Heating rates for January 1992 and July 1992 (Yaws #4 and 9 in Table 1) diagnosed from CLAES and MLS data. The aerosols are not included.

Figure 2. (a) O_3 mixing ratio measured by CLAES (solid line) and MLS (dotted line). The values are given along the top axis. The dashed line is the difference between the CLAES and MLS temperatures, with values given along the bottom axis. (b)-(c) Heating rates derived from: CLAES without aerosols (solid lines), CLAES with aerosols (dashed lines), MLS without aerosols (dotted lines), and MLS with ISAMS aerosols (dash-dotted lines). All profiles are zonal averages at the equator for the January 1992 period (Yaw #4 in Table 1).

Figure 3. The differences in the ozone mixing ratio and temperature measured by the CLAES and MLS instruments and in the derived solar heating and IR cooling rates. The distributions are for (*a*) January 1992 and (*b*) July 1992. The aerosols are not included.

Figure 4. Latitude-height sections of the zonal wind $\bar{u}$.

Figure 5. Latitude-height sections of the mass-weighted streamfunction X^* (in units of 10^9 kg s^{-1}). The contour interval is 0.2 and 1.0 for absolute values lower and greater than 2.0, respectively. The zero-line is thicker and shading denotes areas of counterclockwise flow.

Figure 6. Latitude-height sections of the meridional component of the residual circulation $\bar{v}^*$

Figure 7. Latitude-height sections of the vertical component of the residual circulation $\bar{w}^*$.

Figure 8. Xonally-averaged equatorial time-height sections of (*a*) temperature, (*b*) ozone, (c) zonal wind, (*d*) methane, (*e*) nitrous oxide, and (*f*) $\bar{w}^*$. In panels (a), (*b*), (*d*), and (*e*) the time mean has been taken out. Vertical lines indicate year boundaries.

Figure 9. Latitude-height sections of the momentum residual

Figure lo. The effect of the vertical extinction profile on aerosol heating. All profiles have the same column optical depth of 0.25 and the background atmosphere is the same as in Figure 1 of Gerstell et al. (1995). Blue line: the Gaussian profile used by Gerstell et al. in their Figure 1. Green line: the same profile shifted 2 km to lower altitudes. Yellow' line: a Gaussian profile with a larger half-width. Red line: extinction profile constant with height (as in Kinne et al, 1992).

Figure 11. Extinction profiles and excess aerosol heating derived from co-located CLAES and ISAMS measurements.

Figure 12. The effect of the assumed refractive indices for H_2SO_4-H_2O solutions on the computed aerosol heating rates. The distributions shown are the differences between the case with and without aerosols for the atmosphere characterized by the CLAES measurements during the January 1992 period (Yaw # 4 in Table 1).

Figure 13. Radiative effects of Mt. Pinatubo aerosols at tile equator

Figure 14. Residual vertical velocity at 100 hPa. Solid line: September-October-November (the average for the yaws # 11, 12, 13), dashed line: 1)ecember-January-February (yaws #4, 5, 14) dotted line: March-April-May (yaws # 6, 7, 16, 17), daslled-dotted line: June-July-August (yaws #8, 9, 10). See 'l'able 1 for a list of yaws and their averaging periods.

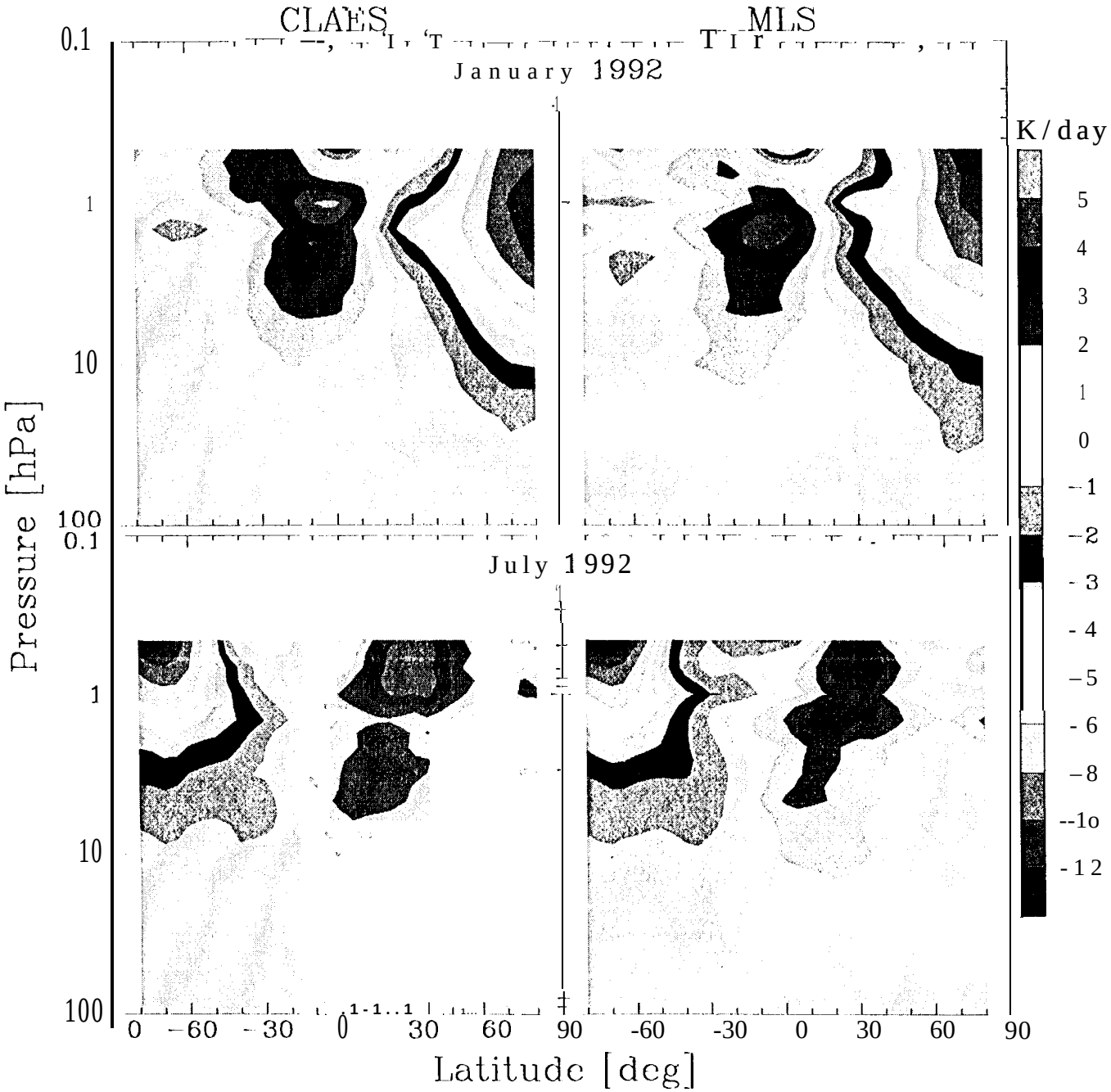
CLAES
MLS
January 1992
July 1992
Pressure [hPa]
0.1
1
10
100
K/day
5
4
3
2
1
0
-1
-2
-3
-4
-5
-6
-8
-10
-12
0
-60
-30
0
30
60
90
Latitude [deg]

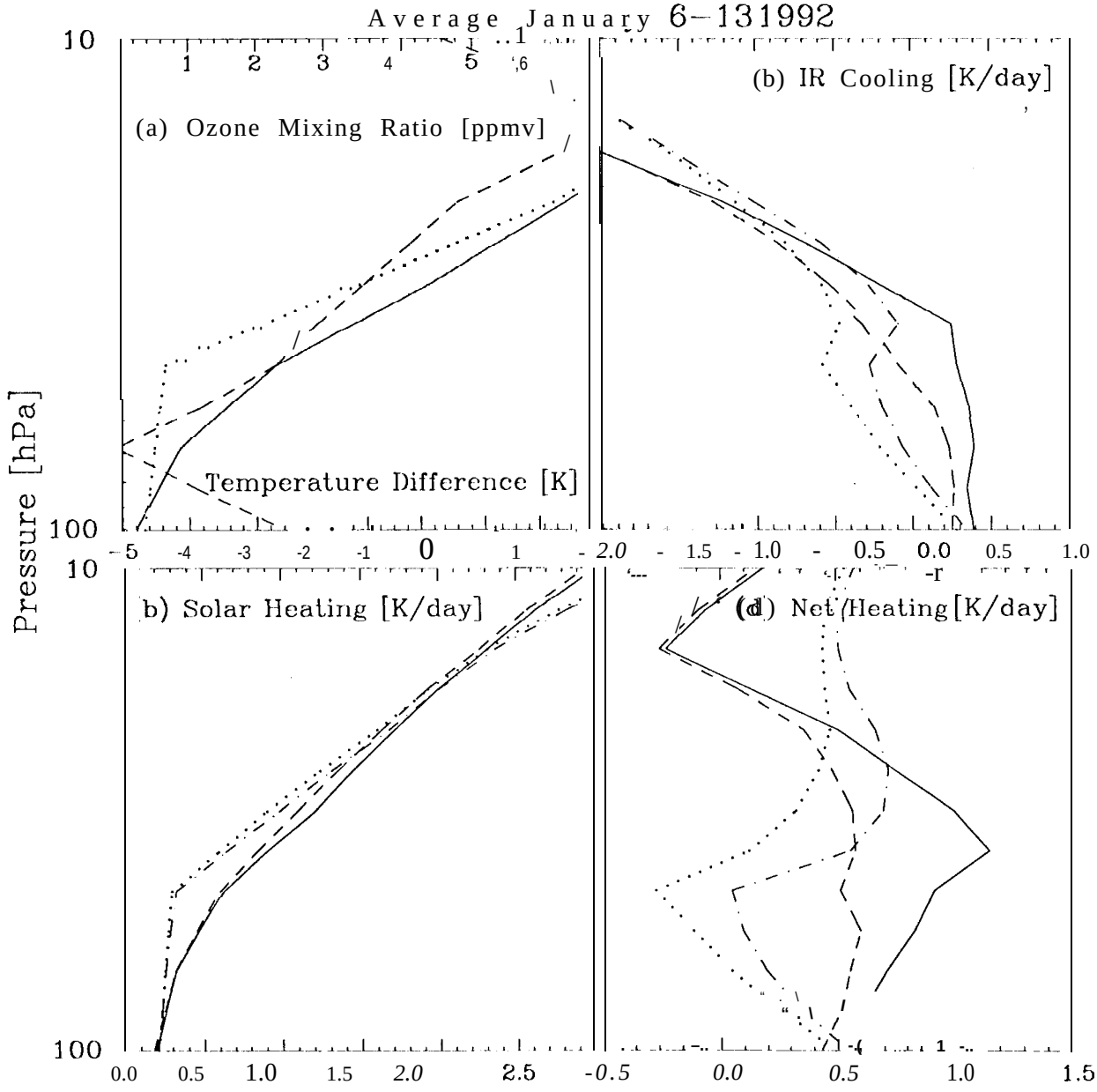
Average January 6–131992
(a) Ozone Mixing Ratio [ppmv]
(b) IR Cooling [K/day]
Temperature Difference [K]
b) Solar Heating [K/day]
(d) Net Heating [K/day]
Pressure [hPa]
10
100
1 2 3 4 5 6
-5 -4 -3 -2 -1 0 1
-2.0 -1.5 -1.0 -0.5 0.0 0.5 1.0
0.0 0.5 1.0 1.5 2.0 2.5
-0.5 0.0 0.5 1.0 1.5

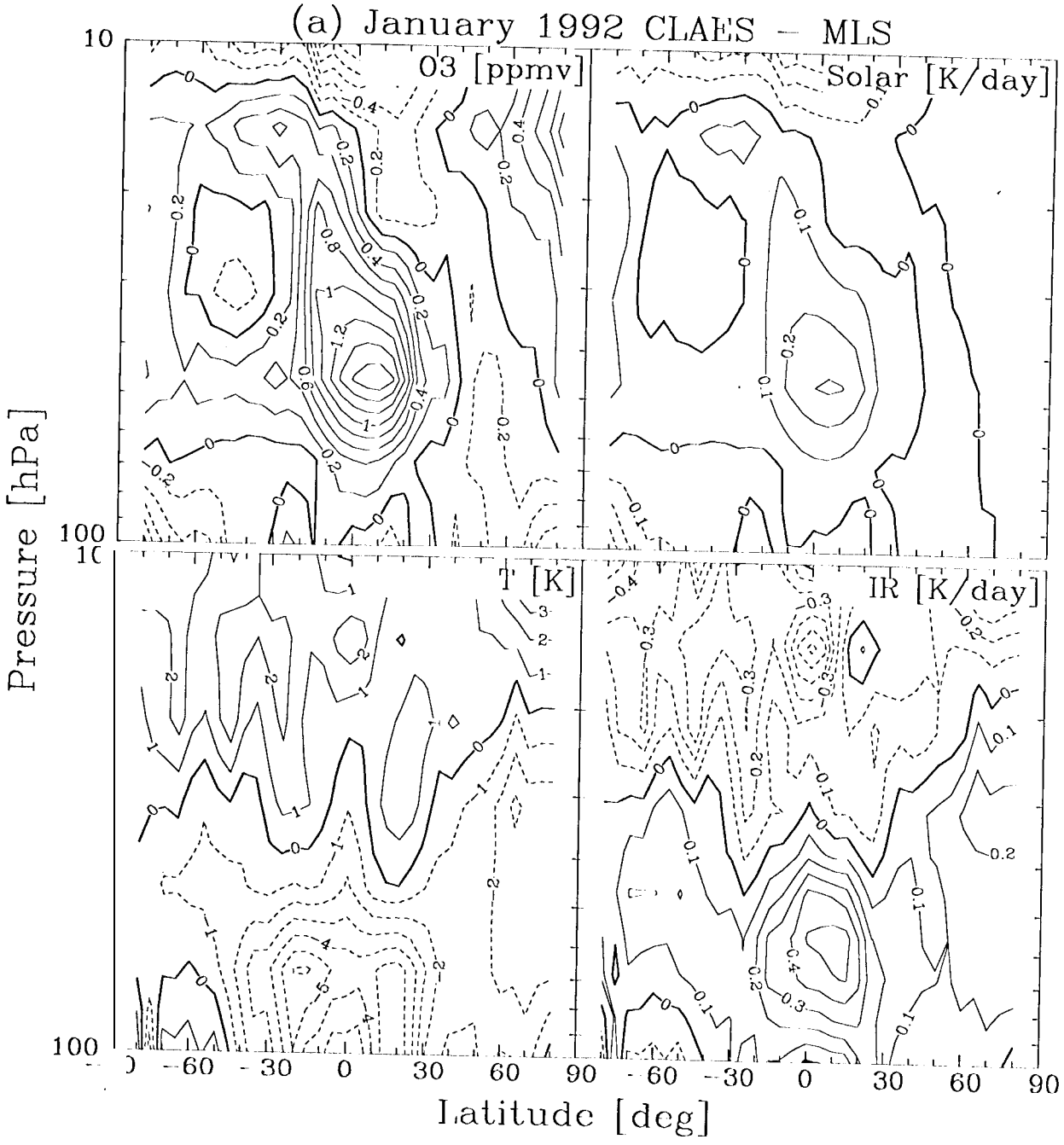
(a) January 1992 CLAES − MLS
O3 [ppmv]
Solar [K/day]
T [K]
IR [K/day]
Pressure [hPa]
10
100
100
-90
-60
-30
0
30
60
90
-60
-30
0
30
60
90
Latitude [deg]

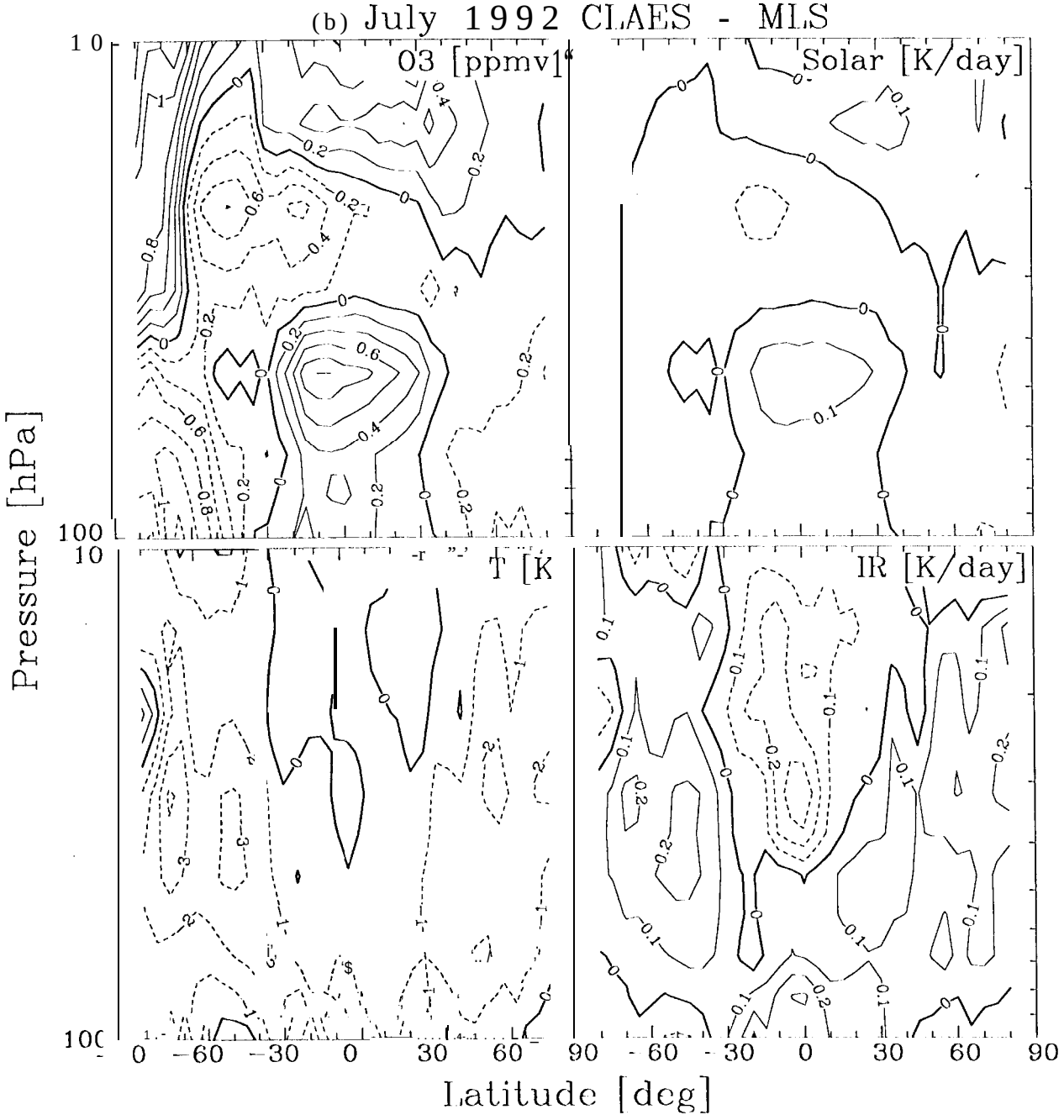
(b) July 1992 CLAES - MLS
O3 [ppmv]
Solar [K/day]
T [K
IR [K/day]
Pressure [hPa]
10
100
10
100
0 -60 -30 0 30 60
90 -60 -30 0 30 60 90
Latitude [deg]

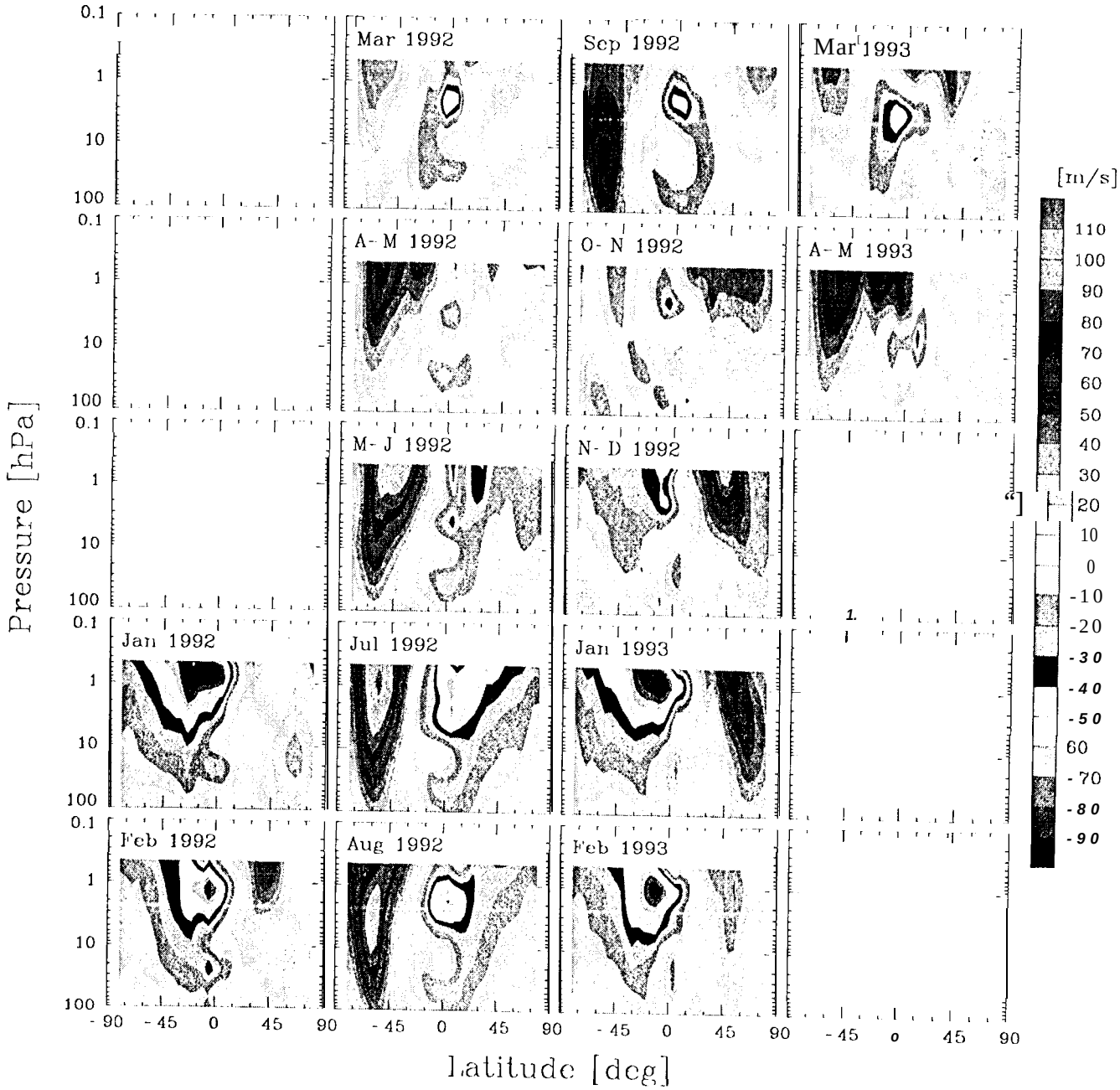
Mar 1992
Sep 1992
Mar 1993
A- M 1992
O- N 1992
A- M 1993
M- J 1992
N- D 1992
Jan 1992
Jul 1992
Jan 1993
Feb 1992
Aug 1992
Feb 1993
Pressure [hPa]
0.1
1
10
100
-90 -45 0 45 90
Latitude [deg]
[m/s]
110
100
90
80
70
60
50
40
30
20
10
0
-10
-20
-30
-40
-50
60
-70
-80
-90

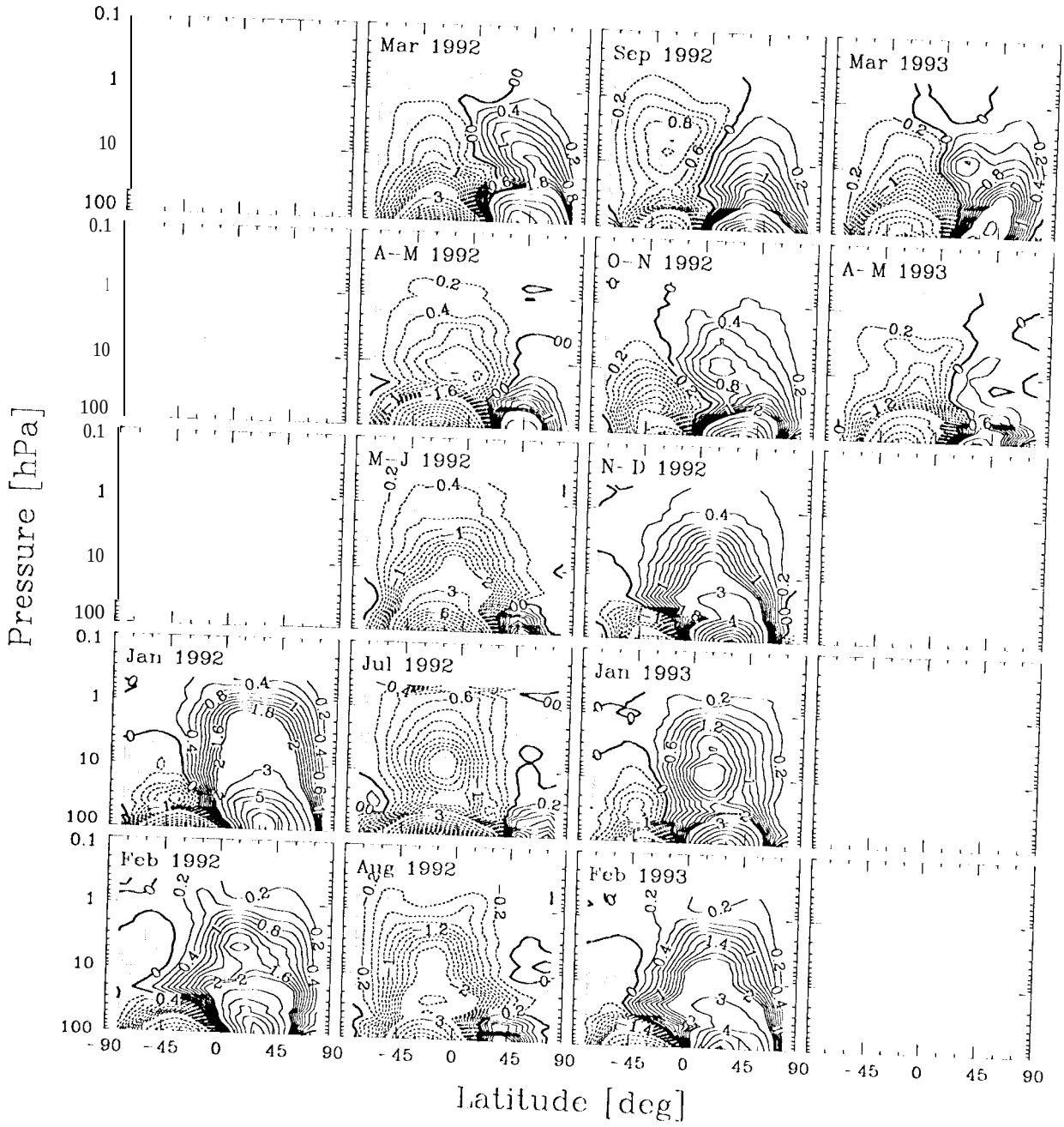
Mar 1992
Sep 1992
Mar 1993
A-M 1992
O-N 1992
A-M 1993
M-J 1992
N-D 1992
Jan 1992
Jul 1992
Jan 1993
Feb 1992
Aug 1992
Feb 1993
Pressure [hPa]
0.1
1
10
100
-90
-45
0
45
90
Latitude [deg]

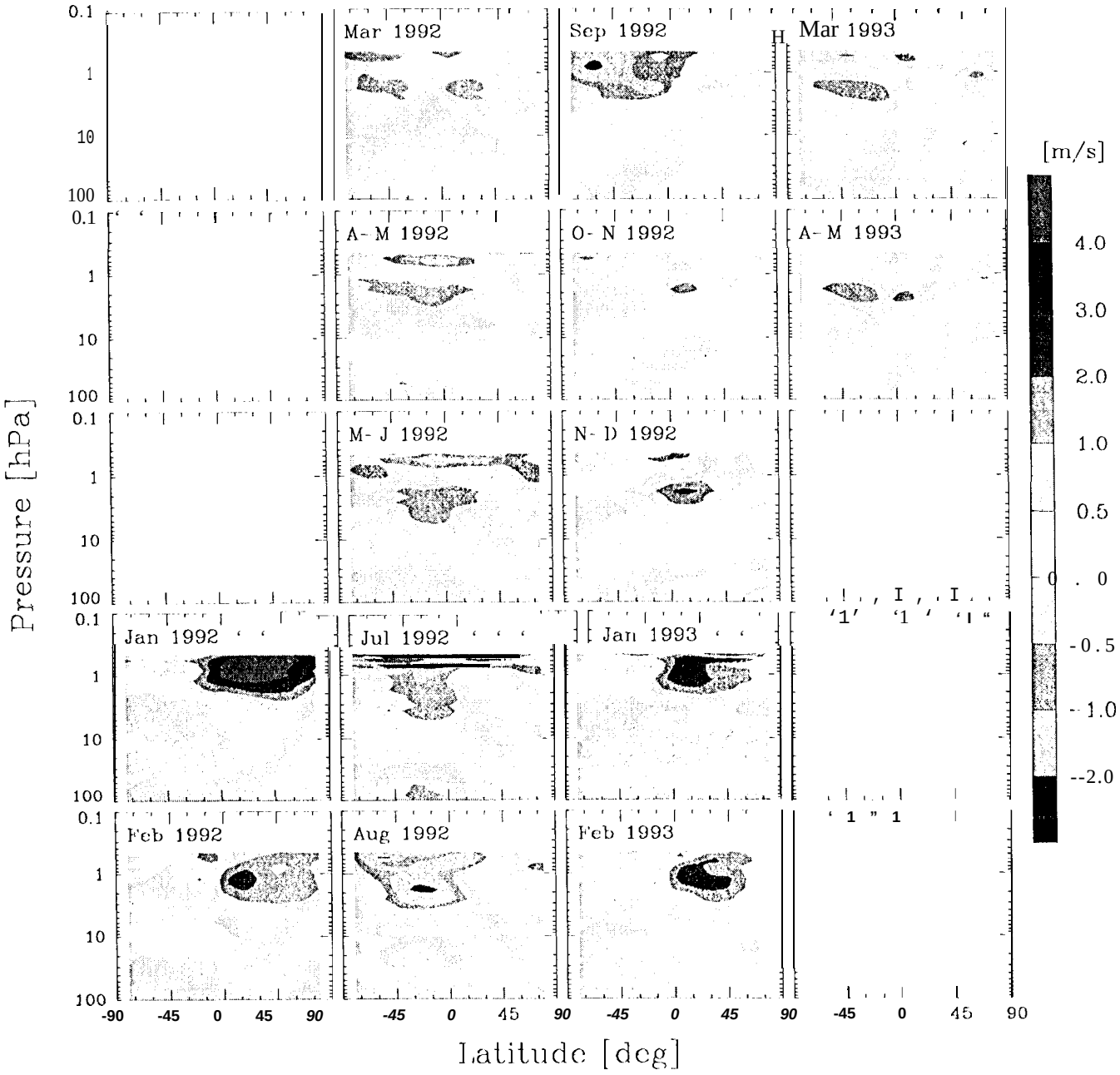
Mar 1992
Sep 1992
Mar 1993
A-M 1992
O-N 1992
A-M 1993
M-J 1992
N-D 1992
Jan 1992
Jul 1992
Jan 1993
Feb 1992
Aug 1992
Feb 1993
Pressure [hPa]
0.1
1
10
100
-90
-45
0
45
90
Latitude [deg]
[m/s]
4.0
3.0
2.0
1.0
0.5
0
-0.5
-1.0
-2.0

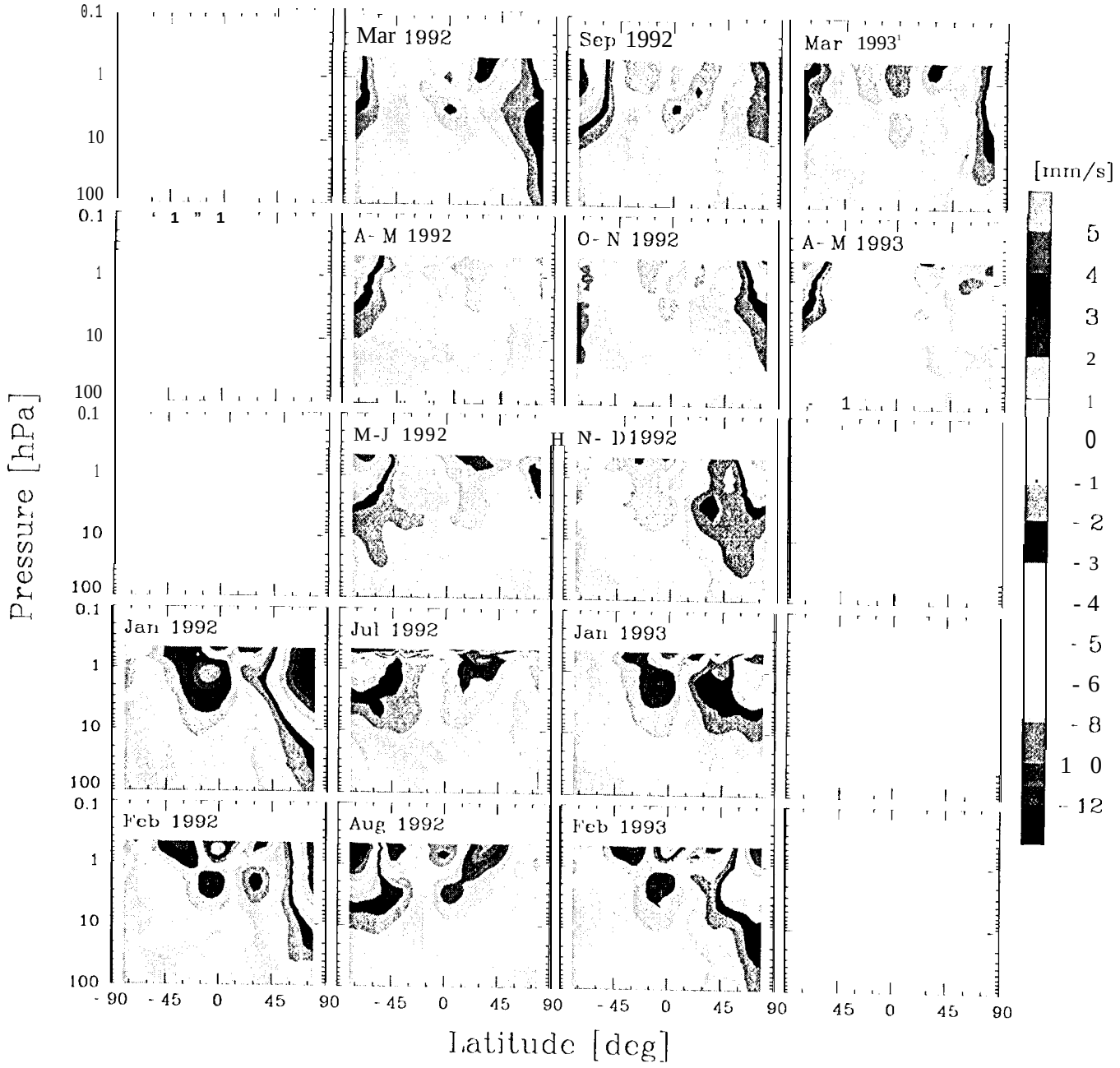
Mar 1992
Sep 1992
Mar 1993
A- M 1992
O- N 1992
A- M 1993
M-J 1992
N- D1992
Jan 1992
Jul 1992
Jan 1993
Feb 1992
Aug 1992
Feb 1993
Pressure [hPa]
0.1
1
10
100
- 90
- 45
0
45
90
Latitude [deg]
[mm/s]
5
4
3
2
1
0
- 1
- 2
- 3
- 4
- 5
- 6
- 8
1 0
- 12

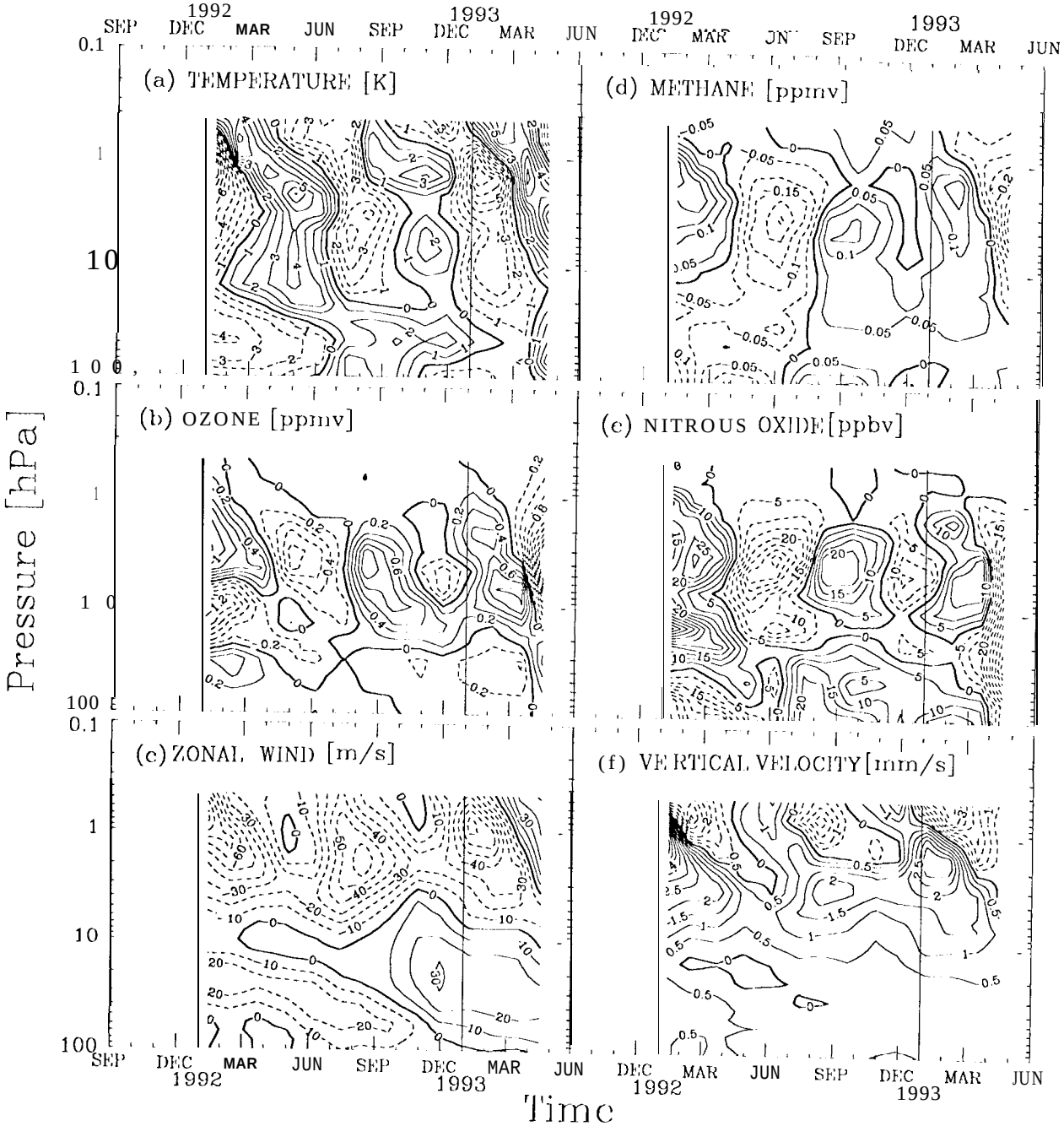
(a) TEMPERATURE [K]
(b) OZONE [ppmv]
(c) ZONAL WIND [m/s]
(d) METHANE [ppmv]
(e) NITROUS OXIDE [ppbv]
(f) VERTICAL VELOCITY [mm/s]
Pressure [hPa]
Time
SEP DEC MAR JUN SEP DEC MAR JUN
1992 1993

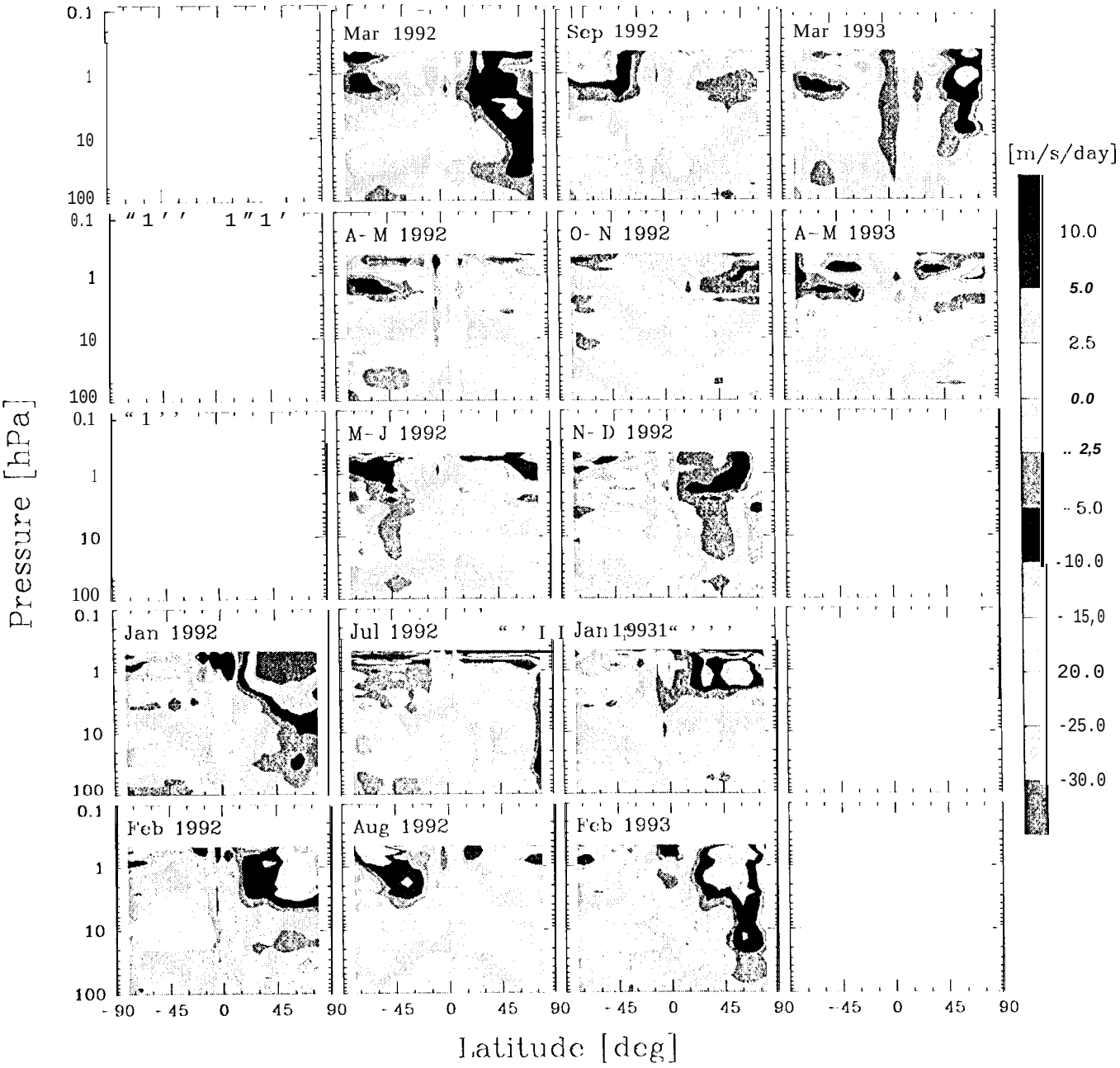
Mar 1992
Sep 1992
Mar 1993
A-M 1992
O-N 1992
A-M 1993
M-J 1992
N-D 1992
Jan 1992
Jul 1992
Jan 1993
Feb 1992
Aug 1992
Feb 1993
Pressure [hPa]
0.1
1
10
100
-90 -45 0 45 90
Latitude [deg]
[m/s/day]
10.0
5.0
2.5
0.0
-2,5
-5.0
-10.0
-15,0
20.0
-25.0
-30.0

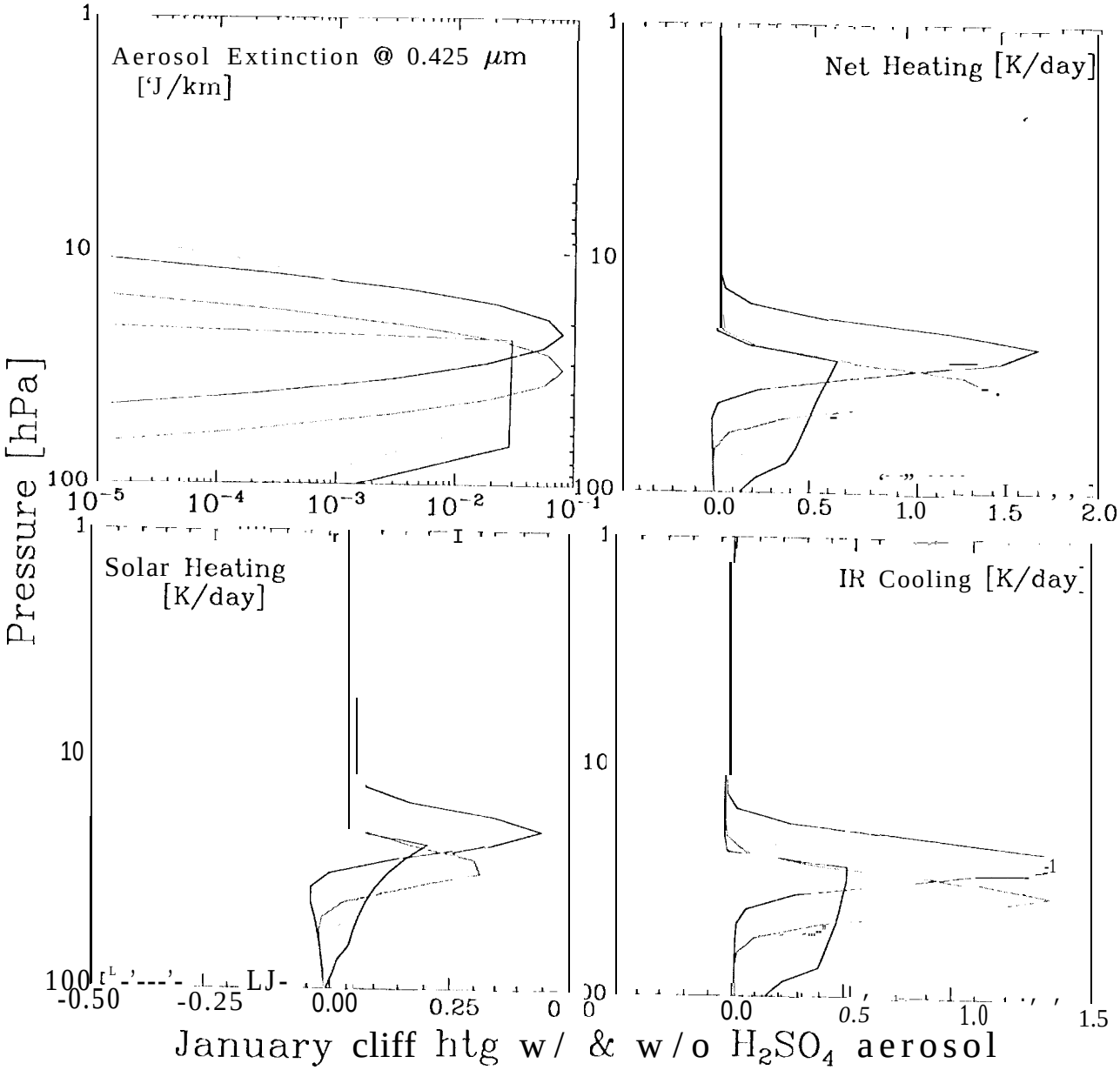
Aerosol Extinction @ 0.425 μm
[1/km]
Net Heating [K/day]
Solar Heating
[K/day]
IR Cooling [K/day]
Pressure [hPa]
1
10
100
10^-5
10^-4
10^-3
10^-2
10^-1
0.0
0.5
1.0
1.5
2.0
-0.50
-0.25
0.00
0.25
0
January cliff htg w/ & w/o H2SO4 aerosol

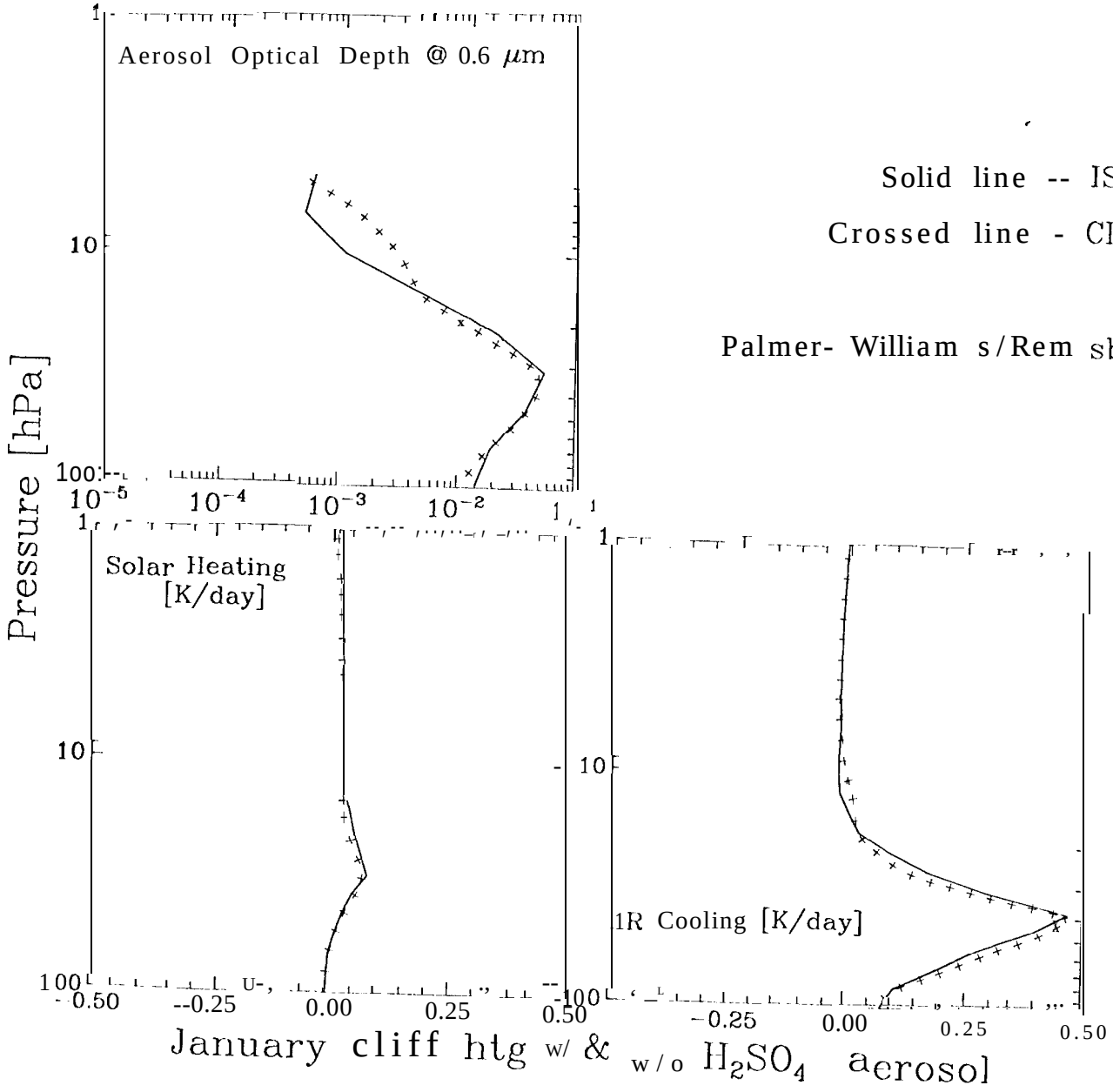
Aerosol Optical Depth @ 0.6 μm
Solid line -- ISAMS
Crossed line - CLAES
Palmer- William s/Rem sberg
Pressure [hPa]
Solar Heating [K/day]
1R Cooling [K/day]
January cliff htg w/ & w/o H_2SO_4 aerosol

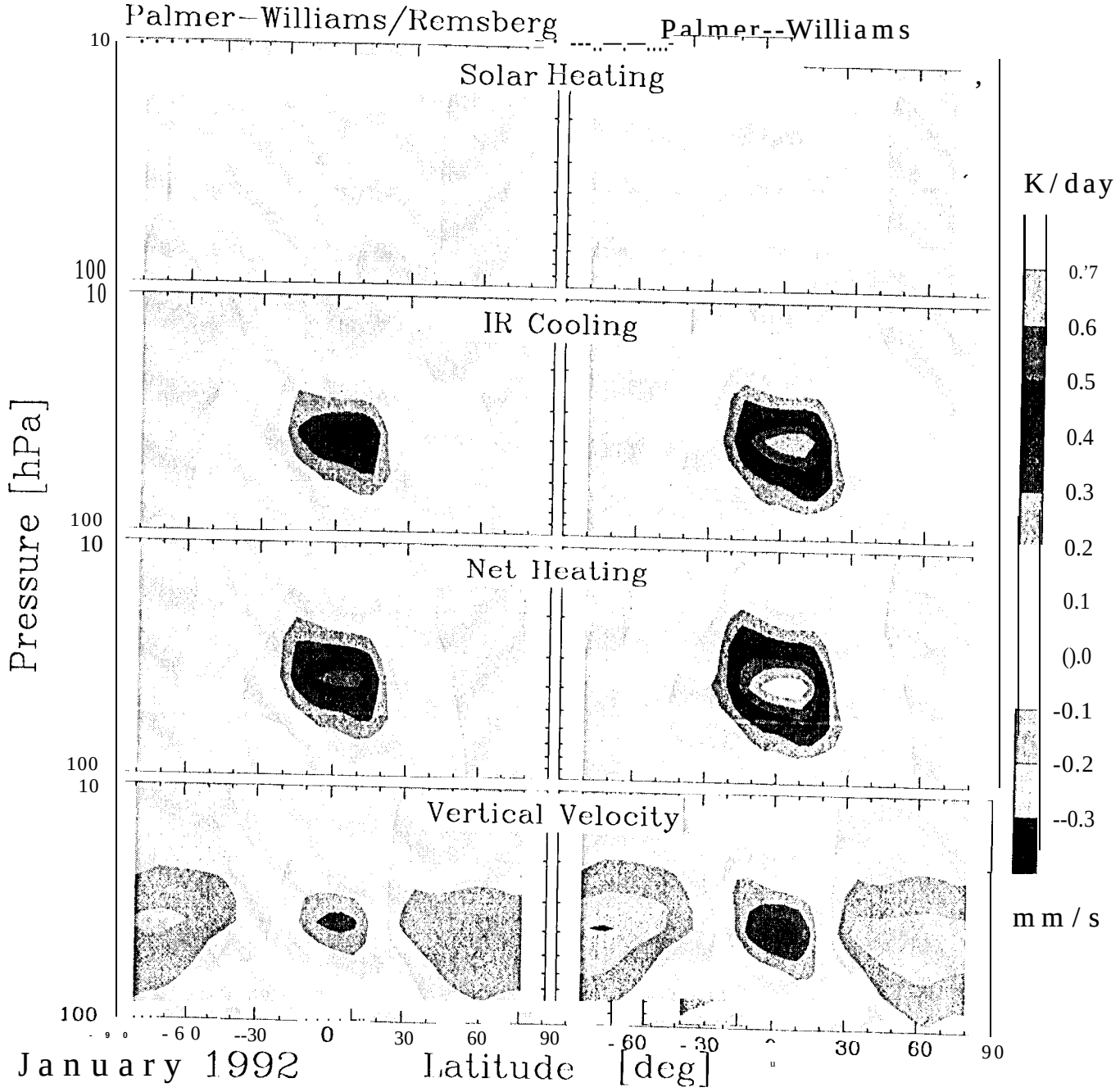
Palmer--Williams/Remsberg
Palmer--Williams
Solar Heating
IR Cooling
Net Heating
Vertical Velocity
Pressure [hPa]
10
100
10
100
10
100
10
100
K/day
0.7
0.6
0.5
0.4
0.3
0.2
0.1
0.0
-0.1
-0.2
-0.3
mm/s
-90
-60
-30
0
30
60
90
-60
-30
30
60
90
January 1992
Latitude [deg]

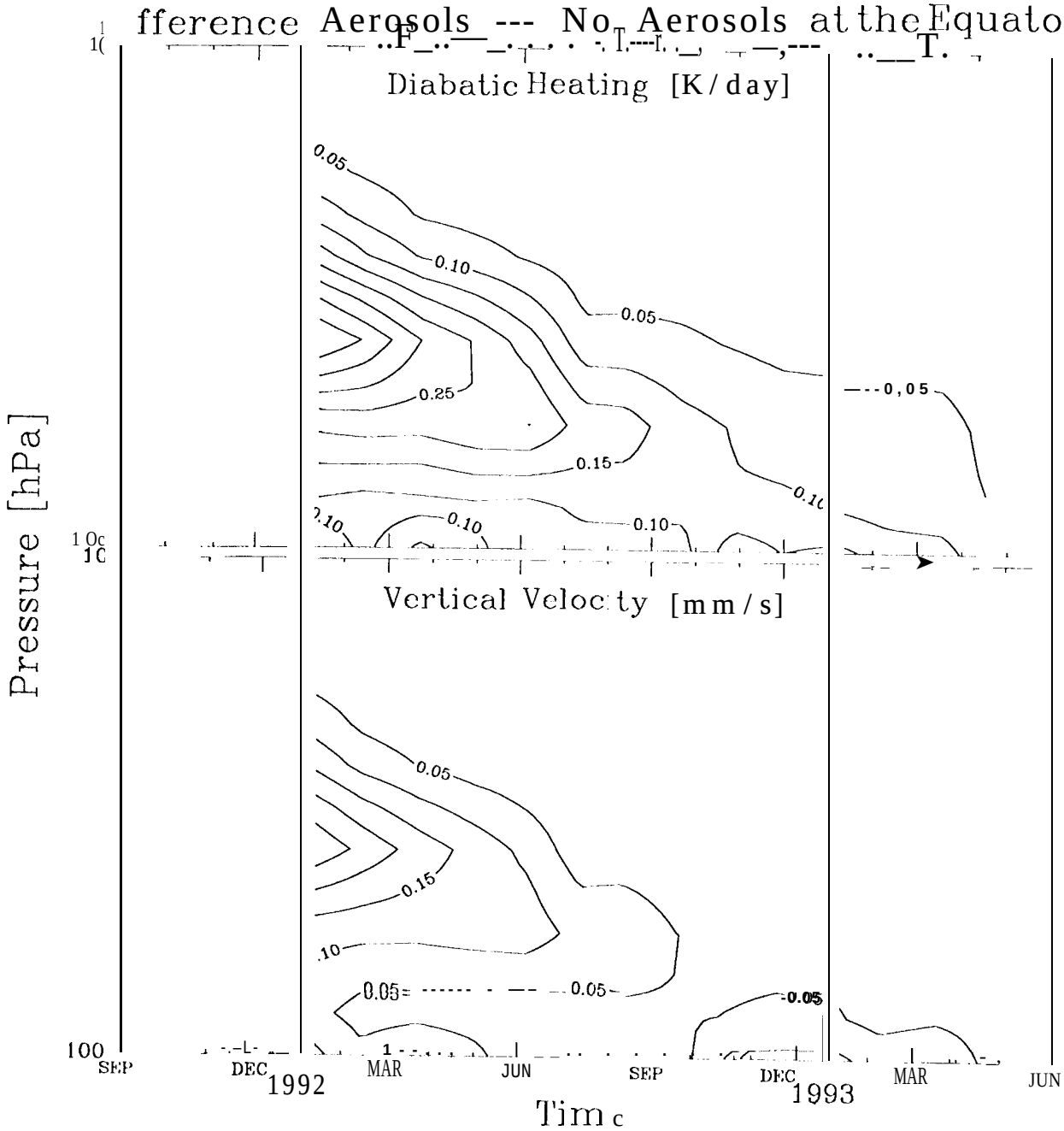
fference Aerosols --- No Aerosols at the Equator
Diabatic Heating [K/day]
0.05
0.10
0.05
0.25
0.15
0.10
0.10
0.10
0.05
0.15
0.05
0.05
0.05
Vertical Velocity [mm/s]
Pressure [hPa]
100
SEP
DEC
1992
MAR
JUN
SEP
DEC
1993
MAR
JUN
Time

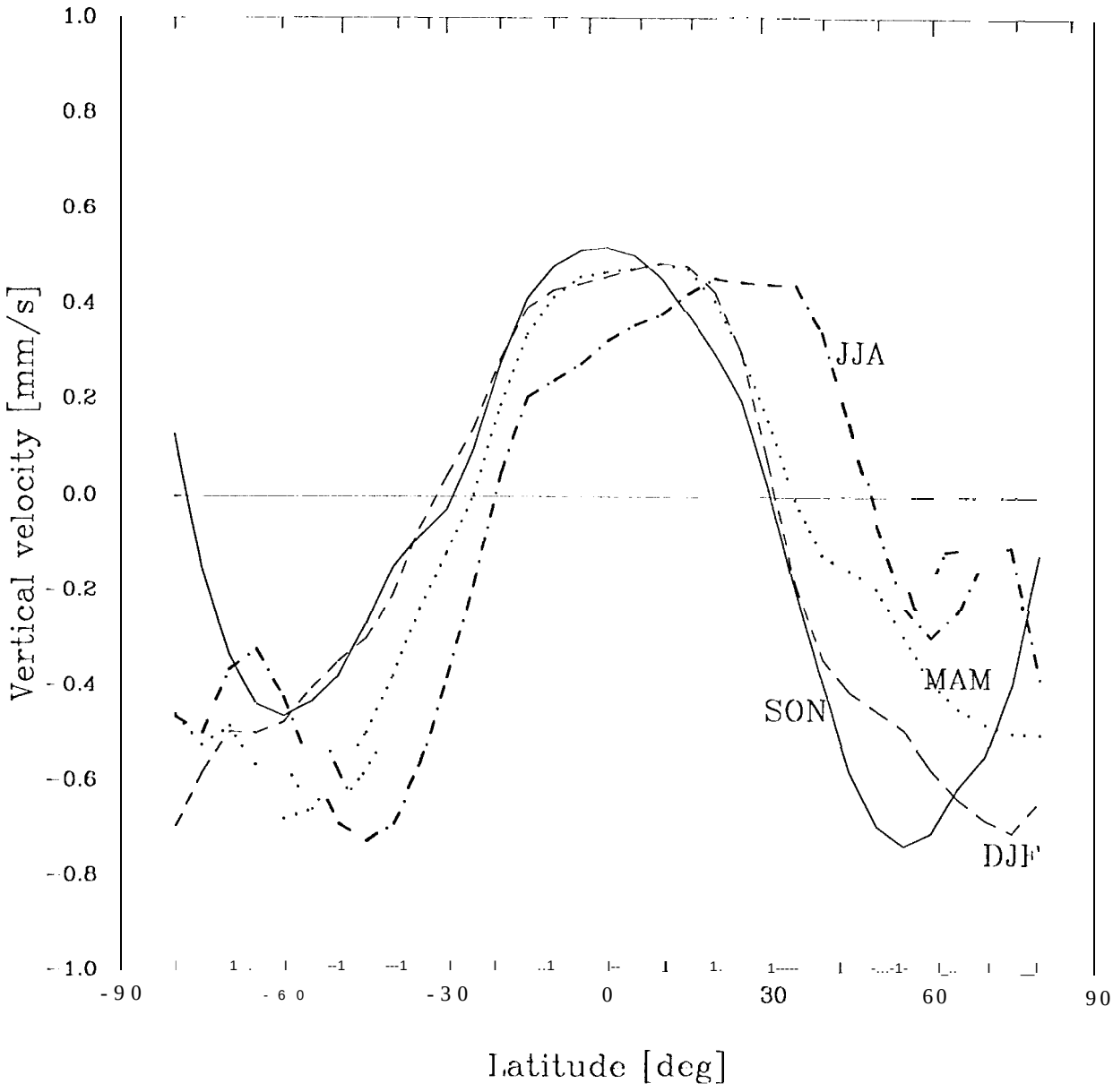
1.0
0.8
0.6
0.4
0.2
0.0
-0.2
-0.4
-0.6
-0.8
-1.0
Vertical velocity [mm/s]
JJA
MAM
SON
DJF
-90
-60
-30
0
30
60
90
Latitude [deg]